# Effect of relative forcing location on separation control with a synthetic jet

**Mark A. Feero & Philippe Lavoie**

Institute for Aerospace Studies
University of Toronto
Toronto, ON, M3H 5T6
Canada
m.feero@mail.utoronto.ca

**Pierre E. Sullivan**

Mechanical and Industrial Engineering
University of Toronto
Toronto, ON, M5S 3G8
Canada

## ABSTRACT

Experiments were conducted to study the effect of synthetic jet control on the post-stall separated flow of a NACA 0025 airfoil at an angle-of-attack of 12° and a Reynolds number of 100,000. In particular, forcing with a single synthetic jet slot located either upstream or downstream of the separation point was studied for several excitation frequencies. Using a decomposition of boundary layer velocity measurements, insight into the effect of control was gained by considering the coherent and turbulent fluctuations. For low-frequency control, coherent fluctuations were contained closer to the wall with downstream excitation as compared with upstream excitation. High-frequency control led to negligible coherent fluctuations and therefore steadily reattached flow.

## INTRODUCTION

Aerodynamic performance degradation of airfoils operating at low Reynolds number is a common issue that is a result of laminar boundary layer separation (Lissaman, 1983). Compared with high Reynolds number flow, the stall angle can be substantially reduced. To mitigate this negative performance, it is desirable to use active flow control techniques to promote flow reattachment. The use of periodic excitation applied locally at the surface to mitigate flow separation on stalled airfoils is a technique that has been applied with varying degrees of success for a number of years (Glezer, 2011). A common device for applying such control is the synthetic jet; a zero-net-mass-flux (ZNMF) device that uses the working fluid to impart unsteady momentum on the flow.

Important control parameters for ZNMF control include excitation frequency, excitation amplitude and actuator geometry. The former two parameters are often characterized by the reduced frequency, $F^+ = f_e c/U_\infty$, and the blowing ratio, $C_B = \overline{U_j}/U_\infty$ (where $f_e$ is excitation frequency, $c$ is chord length, $U_\infty$ is freestream velocity and $\overline{U_j}$ is the mean expulsion velocity of the jet). The actuator geometry is more complex and may include parameters such as the jet injection angle, chordwise location, shape (i.e., slot(s) or orifices), etc. While the effects of $F^+$ and $C_B$ have received considerable attention (e.g., Amitay & Glezer (2002), Seifert *et al.* (1996)), the effect of excitation location on control is much less studied. Some authors suggest that forcing should be applied as close to separation as possible (Greenblatt & Wygnanski, 2000), but this has yet to be shown conclusively, nor has it been addressed whether forcing upstream or downstream of separation is more effective for control.

The goal of the present work was to study experimentally the effects of synthetic jet control applied at locations equidistant upstream and downstream of the separation point on a post-stalled airfoil at low Reynolds number. Two excitation frequencies were considered: $F^+ = 1$ and 58, for "low-frequency" and "high-frequency" control, respectively. Control effectiveness was investigated by section lift coefficient measurements over a large range of blowing ratios. Insight into the effect of the control on the reattached flow was gained from boundary layer velocity measurements, including decomposition of the fluctuations into coherent and turbulent components.

## EXPERIMENTAL SETUP

Experiments were performed in a low-speed recirculating wind tunnel located at the University of Toronto. Flow enters a test section that is 0.9 m wide and 1.2 m tall after passing through flow conditioning consisting of seven screens and a 12:1 contraction. The turbulence intensity at the test section inlet is 0.08% over a frequency band from 0.5 Hz to 10 kHz. The freestream velocity is monitored by a pitot-static tube located at the test section entrance. The experiments in the current study were performed at $Re_c = 100{,}000$, which corresponds to a freestream velocity of approximately $U_\infty = 5$ m/s. The airfoil model has a NACA 0025 cross-section, a chord length $c = 300$ mm and a spanwise length of 885 mm. A chordwise row of 64 pressure taps is distributed between the upper and lower surfaces at midspan. End plates mounted to the ends of the model to isolate the model from the tunnel wall boundary layer and promote spanwise uniformity of the baseline flow.

A synthetic jet actuator with a single 0.5 mm by 294 mm slot was installed in the suction surface of the airfoil. To vary the chordwise location of the slot while maintaining an angle normal to the surface, a modular insert housing the slot was replaced for each desired location. The present work examines two slot locations: $x_j/c = 0.09$ and 0.17, where $x_j$ is the chordwise distance from the leading edge of the jet, as shown in Figure 1. The synthetic jet cavity is driven by 16 piezoelectric disks operating in phase. At an excitation frequency of $f_e = 1000$ Hz, the mean expulsion velocity of the jet can be increased to approximately 16 m/s at the maximum input voltage. For each slot location, a bench-top calibration of the synthetic jet velocity was performed prior to the wind tunnel experiments. Excitation at $f_e = 1000$ Hz corresponds to $F^+ = 58$ and therefore serves as high-frequency control. To achieve $F^+ = 1$ for low-frequency control, the sinusoidal carrier wave at 1000 Hz was burst modulated (i.e., modulated by a square wave varying between 0 and 1) at approximately 17 Hz. The duty cycle of the modulated signal was fixed at 50%.

Boundary layer velocity measurements were performed using hot-wire anemometry. The position of a single-wire, boundary-layer-type probe with 5μm diameter was controlled by a streamlined traverse with a solid blockage less than 2% (shown in Figure 1). The hot-wire was held at the end of an arm extending 400 mm from the traverse and the angle of the probe relative to the surface was maintaned less than 10° (Brendel & Mueller, 1988). The hot-wire was calibrated in situ and a King's Law fit was used to evaluate velocities below the calibration range. The measurement uncertainty due to calibration for mean and RMS velocities is approximately ±1% (Yavuzkurt, 1984). Mean and RMS velocities were converged to within 0.2 m/s ($0.04U_\infty$) at the 95% confidence interval.

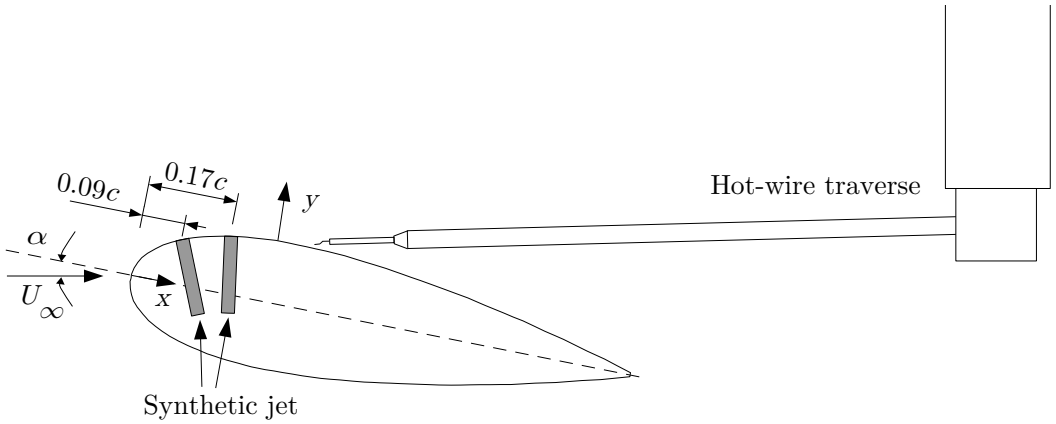


Figure 1: Schematic of the wind tunnel setup showing the synthetic jet positions within the airfoil and the traverse for boundary layer velocity measurements. The chordwise and wall-normal coordinates $x$ and $y$, respectively, are also defined.

## RESULTS

The baseline flow at $Re_c = 100,000$ and $\alpha = 12^\circ$ is stalled with laminar boundary layer separation occurring near the leading edge. The baseline pressure coefficient distribution, $C_p = (p - p_\infty)/q_\infty$ (where $p$ is mean static pressure, and $p_\infty$ and $q_\infty$ are the mean freestream static and dynamic pressure, respectively), is shown in Figure 2. Stalled flow is indicated by the region of approximately constant $C_p$ on the suction surface extending to the trailing edge. The beginning of this constant pressure region marks the separation point, which is $x_s = 0.13$. This was also confirmed from boundary layer profiles measured by hot-wire. The two selected slot locations, $x_j = 0.09$ and $x_j = 0.17$, therefore correspond to locations upstream and downstream, respectively, of the mean separation point. A normalized actuation location based on separation is defined as $x_j^* = (x_j - x_s)/c$. The normalized synthetic jet slot locations are $x_j^* = -4.3\%$ and $x_j^* = 4.3\%$.

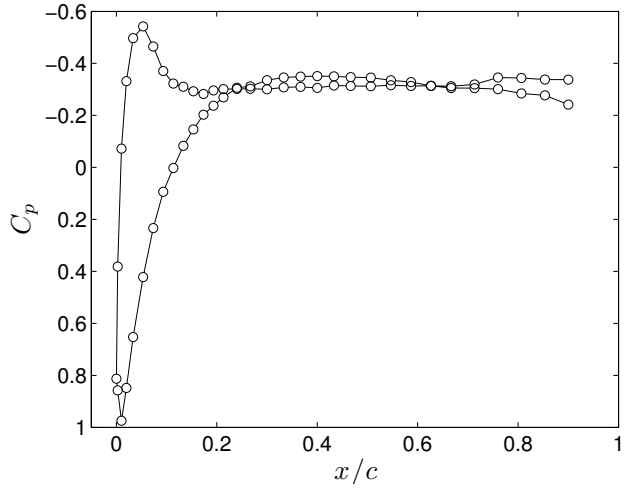


Figure 2: Baseline surface pressure distribution at $Re_c = 100,000$ and $\alpha = 12^\circ$.

Pressure coefficient distributions for the flow conditions described above were measured for each slot location to determine the state of the flow over the airfoil and the section lift coefficient at midspan as $C_B$ was increased for $F^+ = 1$ and $F^+ = 58$. The lift coefficient, $C_L$, for each of the four cases as a function of $C_B$ is presented normalized by the baseline lift coefficient $C_{Lo} = 0.135 \pm 0.004$ in Figure 3a. The general trend shows that as $C_B$ is increased above a certain value, $C_L$ increases towards an upper limit until the effect of increasing $C_B$ saturates. At $x_j^* = -4.3\%$, even the lowest blowing ratios tested had a positive effect, while at $x_j^* = 4.3\%$ there was no lift increase until $C_B = 1$ for $F^+ = 1$, and $C_B = 1.5$ for $F^+ = 58$. At $x_j^* = 4.3\%$ and $F^+ = 58$, the blowing ratio could not be increased to a point where saturation was observed. Since substantially larger $C_B$ was required at $x_j^* = 4.3\%$ for flow reattachment, a threshold blowing ratio was defined to normalize $C_B$. This threshold, $C_B{}^*$, was defined as the value of $C_B$ required to cause fully attached flow over the suction surface for all $F^+$ at a given slot location. This is in contrast to values of $C_B$ less than $C_B{}^*$ that either have no effect on the flow, or create a laminar separation bubble (LSB) in the time-averaged sense. Fully attached flow was determined from the shape of the $C_p$ profile. This was used to estimate $C_B{}^*$ and guide subsequent hot-wire boundary layer measurements, which in some cases revealed a small LSB where fully attached flow was presumed. The threshold blowing ratio for $x_j^* = -4.3$ and 4.3 were estimated as $C_B{}^* = 0.8$ and 2, respectively. The $C_p$ distributions at $C_B/C_B{}^* = 1$ are shown in Figure 4. Note that gaps in the data are due to missing pressure taps at the synthetic jet location. Despite the large region of relatively low pressure gradient for $F^+ = 58$ and $x_j^* = 4.3\%$, boundary layer measurements confirmed attached flow over the suction surface. The lift coefficient data is also presented as a function of $C_B/C_B{}^*$ in Figure 3b. With upstream forcing at $x_j^* = -4.3\%$, $C_B/C_B{}^* = 1$ approximately corresponds to the point where increasing $C_B$ no longer produces additional increase in $C_L$. This is not the case with downstream forcing at $x_j^* = 4.3\%$, particularly for $F^+ = 58$. The effect of control on the flow at $C_B/C_B{}^* = 1$ for each slot location and frequency is examined further using velocity measurements.

Boundary layer velocity measurements were performed over the suction surface downstream of the synthetic jet for each of the four control cases shown in Figure 4. To study the effect of control on the flow, a triple decomposition was used to extract the coherent and turbulent velocity fluctuations (Hussain & Reynolds, 1970), *viz*:

$$u(t) = U + \tilde{u}(t) + u'(t), \tag{1}$$

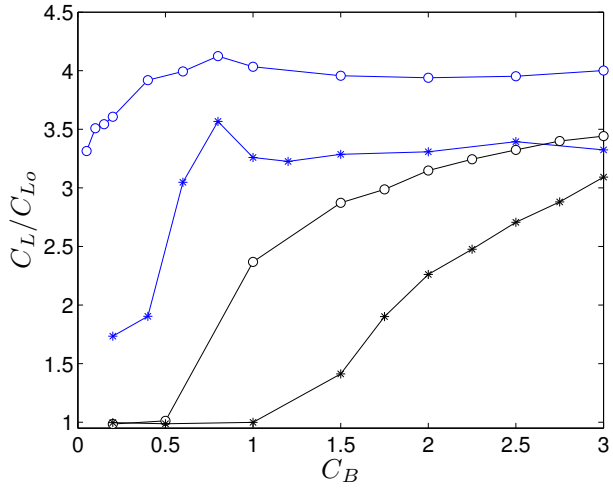


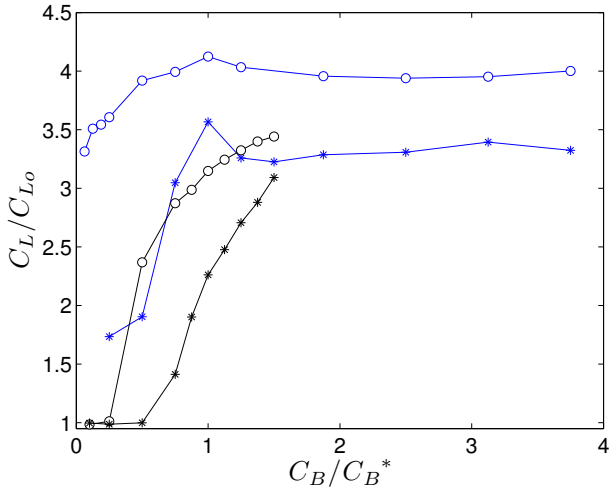


Figure 3: Lift coefficient increment as a function of $C_B$ and $C_B/C_B{}^*$. ($\circ$) $F^+ = 1$, ($*$) $F^+ = 58$. Blue lines: $x_a^* = -4.3\%$, black lines: $x_a^* = 4.3\%$.

where $U$ is the time-averaged velocity, $\tilde{u}$ is the coherent component and $u'$ is the random turbulent component. The phase-averaged velocity is defined as:

$$\langle u(t) \rangle = \frac{1}{N} \sum_{i=0}^{N} u(t + i \cdot T), \tag{2}$$

where $N$ is the number of cycles and $T$ is the period of the control signal. The turbulent component is given by $u'(t) = u(t) - \langle u(t) \rangle$.

The effect of control on the mean flow can be compared to the baseline flow by considering the evolution of the displacement thickness, $\delta^*$, over $x/c = 0.2 - 0.9$. Displacement thickness is computed from profiles of $U$, *viz.*

$$\delta^* = \int_0^\infty \left(1 - \frac{U}{U_e}\right) \mathrm{d}y, \tag{3}$$

where $U_e$ is the local edge velocity. Figure 5 shows $\delta^*$ over the suction surface for the baseline flow and the four control cases shown in

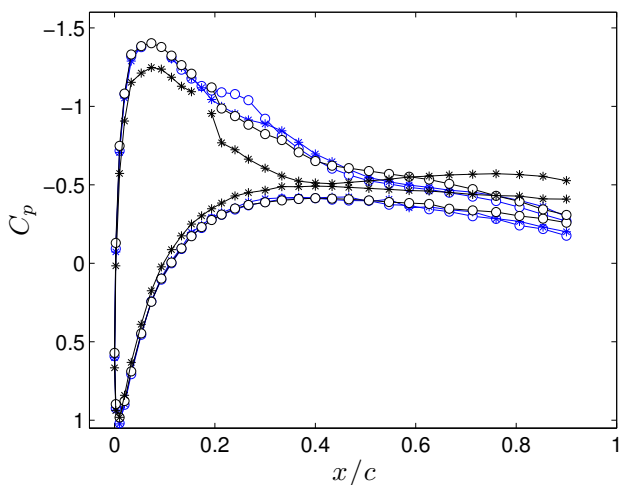


Figure 4: Surface pressure distributions at $C_B/C_B^* = 1$. ($\circ$) $F^+ = 1$, ($*$) $F^+ = 58$. Blue and black symbols indicate $x_a^* = -4.3\%$ and $4.3\%$, respectively.

Figure 4. It should be noted that $\delta^*$ for the baseline flow is underestimated due to rectification of the reversed flow, with the error likely on the order of 10% – 20% (Brendel & Mueller, 1988; Fitzgerald & Mueller, 1990). In each case, the attached flow with control is marked by a substantial reduction in $\delta^*$ over the entire measurement domain. A reduction by nearly a factor of 10 is observed for $F^+ = 1$ and $x_j^* = -4.3\%$. Comparing Figures 3b and 5, the results show that $\delta^*$ near the trailing edge at $x/c = 0.9$ follows the inverse trend of $C_L$ at $C_B/C_B^* = 1$. That is, despite each case having fully attached flow, a thinner boundary layer near the trailing edge (i.e., lower $\delta^*$) corresponds to larger $C_L$.

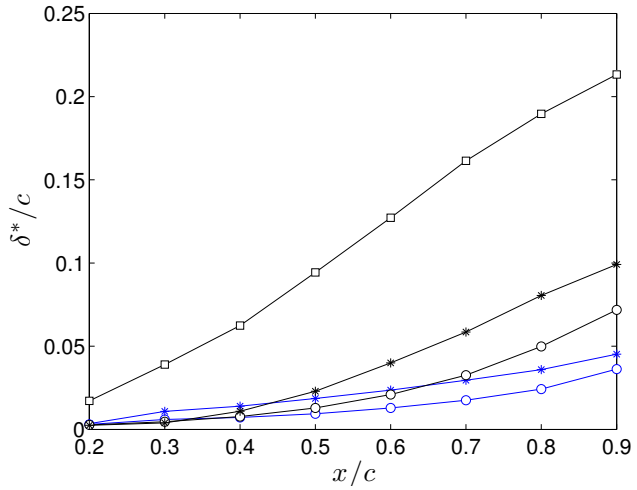


Figure 5: Chordwise variation in displacement thickness for the baseline and control cases at $C_B/C_B^* = 1$. Markers are the same as Fig. 4, with the addition of ($\square$) for the baseline case.

The evolution of the RMS velocity, $u'_{\mathrm{rms}}$, over the suction surface for the baseline flow is provided as reference for the control

cases. Figure 6 shows the $u'_{\rm rms}$ profiles normalized by $U_\infty$ over $x/c = 0.2$ – 0.9. The wall-normal coordinate, $y$, has been normalized by the local 99% boundary layer thickness, $\delta$, to account for the drastic boundary layer growth along the chord (see Figure 5). Over this chordwise range, $u'_{\rm rms}$ grows from approximately $0.1U_\infty$ to $0.2U_\infty$. The width of the peak in $u'_{\rm rms}/U_\infty$ becomes wider as $x$ increases along the chord and the separated shear layer becomes thicker.

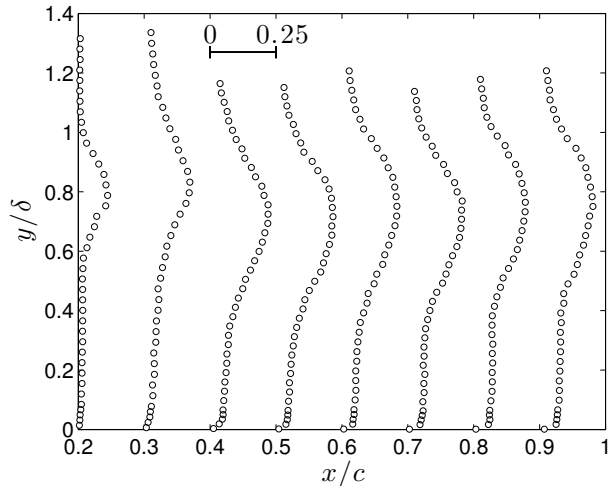


Figure 6: Profiles of $u'_{\rm rms}/U_\infty$ for the baseline flow. Scale shown at the top of the plot.

Figure 7 shows the coherent and turbulent RMS velocity profiles for the four control cases at $C_B/{C_B}^* = 1$. The results for $F^+ = 1$ will first be considered. When forcing is applied upstream of separation at $x_j^* = -4.3\%$, the magnitude of the coherent and turbulent fluctuations are similar, until $x/c \geq 0.7$ where the turbulent fluctuations begin to dominate. This is in exception to $x/c = 0.2 - 0.3$ (near the jet location) where there are substantial coherent fluctuations throughout the boundary layer. For forcing at $x_j^* = 4.3\%$, in the region close to excitation, the magnitude of the coherent fluctuations near the wall are much larger and they dominate over the turbulent fluctuations. Once $x/c = 0.5$ is reached, $u'_{\rm rms}$ begins to dominate and become larger than $\tilde{u}_{\rm rms}$ through most of the boundary layer. Compared with $x_a^* = -4.3\%$, there is greater turbulent energy away from the wall, with a broad peak in $u'_{\rm rms}$ observed at $x/c > 0.5$ and its maximum located near $y/\delta \approx 0.5$. This broad distribution of larger turbulent fluctuations in the boundary layer coincides with a larger $\delta^*$ for downstream forcing at $F^+ = 1$. For each forcing location, the coherent fluctuations suggest the passage of a vortical structure over the airfoil throughout the cycle.

The behaviour for $F^+ = 58$ is substantially different than $F^+ = 1$ in that for each forcing location, the coherent fluctuations are negligible (except nearest the synthetic jet for $x_a^* = 4.3\%$). This is indicative of flow that is steadily attached. When forcing is applied upstream, there are larger turbulent fluctuations in the outer part of the boundary layer for $x/c \leq 0.5$ compared with the downstream case. There is also a rapid growth of the fluctuations, as can be seen by comparing the $u'_{\rm rms}$ profiles at $x/c = 0.2$ and 0.3 for $x_a^* = -4.3\%$. At $x/c = 0.2$ the magnitude of the fluctuations for the downstream forcing case is much larger, likely associated with the fact that the blowing ratio necessary for reattachment is significantly larger than the upstream case. Similar to forcing at $F^+ = 1$, a broader distribution of $u'_{\rm rms}$ with a maximum near $y/\delta \approx 0.5$ is observed near the trailing edge for $x_j^* = 4.3\%$, whereas a larger peak near the wall is present for $x_j^* = -4.3\%$. This is consistent with a larger trailing edge displacement thickness for $x_j^* = 4.3\%$ than $x_j^* = -4.3\%$ with forcing at $F^+ = 58$.

## CONCLUSIONS

Synthetic jet control on a post-stall NACA 0025 airfoil at $Re_c = 100{,}000$ and $\alpha = 12^\circ$ was studied with an emphasis on comparing excitation locations upstream and downstream of the separation point. With the synthetic jet at an equal chordwise distance downstream of separation, a substantially larger threshold blowing ratio was required to cause fully attached flow compared with upstream forcing. The threshold blowing ratios were ${C_B}^* = 0.8$ and 2 for the upstream and downstream forcing locations, respectively. Boundary layer velocity measurements were compared for $F^+ = 1$ and 58 at each excitation location with a constant blowing ratio relative to the threshold, $C_B/C_B^* = 1$. The displacement thickness computed from mean velocity profiles showed a trend consistent with $C_L$; i.e., lower $\delta^*$ near the trailing edge coincided with larger $C_L$. The velocity fluctuation decomposition demonstrated that for $F^+ = 1$, there were substantial coherent velocity fluctuations throughout the boundary layer in the upstream forcing case, while with downstream forcing the coherent fluctuations were contained much closer to the wall. Unlike $F^+ = 1$, at $F^+ = 58$ the coherent fluctuations were negligible, consistent with steadily attached flow. In the upstream forcing case, there was an initial rapid growth of turbulent fluctuations in the outer region of the boundary layer, however towards the trailing edge a peak near the wall emerged and dominated. A similarity between $F^+ = 1$ and $F^+ = 58$ was observed for downstream forcing where a broad peak in turbulent fluctuations with its maximum near $0.5\delta$ developed near the trailing edge.

## REFERENCES


Amitay, Michael & Glezer, Ari 2002 Role of actuation frequency in controlled flow reattachment over a stalled airfoil. *AIAA Journal* **40** (2), 209–216.

Brendel, M. & Mueller, T. J. 1988 Boundary-Layer Measurements on an Airfoil at Low Reynolds Numbers. *J. Aircraft* **25** (7), 612–617.

Fitzgerald, Edward J & Mueller, Thomas J 1990 Measurements in a separation bubble on an airfoil using laser velocimetry. *AIAA journal* **28** (4), 584–592.

Glezer, A. 2011 Some aspects of aerodynamic flow control using synthetic-jet actuation. *Philosophical Transactions of the Royal Society A: Mathematical, Physical and Engineering Sciences* **369** (1940), 1476–1494.

Greenblatt, D. & Wygnanski, I. J. 2000 The control of flow separation by periodic excitation. *Progress in Aerospace Sciences* **36** (7), 487–545.

Hussain, A. K. M. F. & Reynolds, W. C. 1970 The mechanics of an organized wave in turbulent shear flow. *Journal of Fluid Mechanics* **41** (02), 241–258.

Lissaman, P. B. S. 1983 Low-Reynolds-number airfoils. *Annual Review of Fluid Mechanics* **15**, 223–239.

Seifert, A., Darabi, A. & Wyganski, I. J. 1996 Delay of airfoil stall by periodic excitation. *Journal of Aircraft* **33** (4), 691–698.

Yavuzkurt, S. 1984 A guide to uncertainty analysis of hot-wire data. *ASME Transactions Journal of Fluids Engineering* **106**, 181–186.

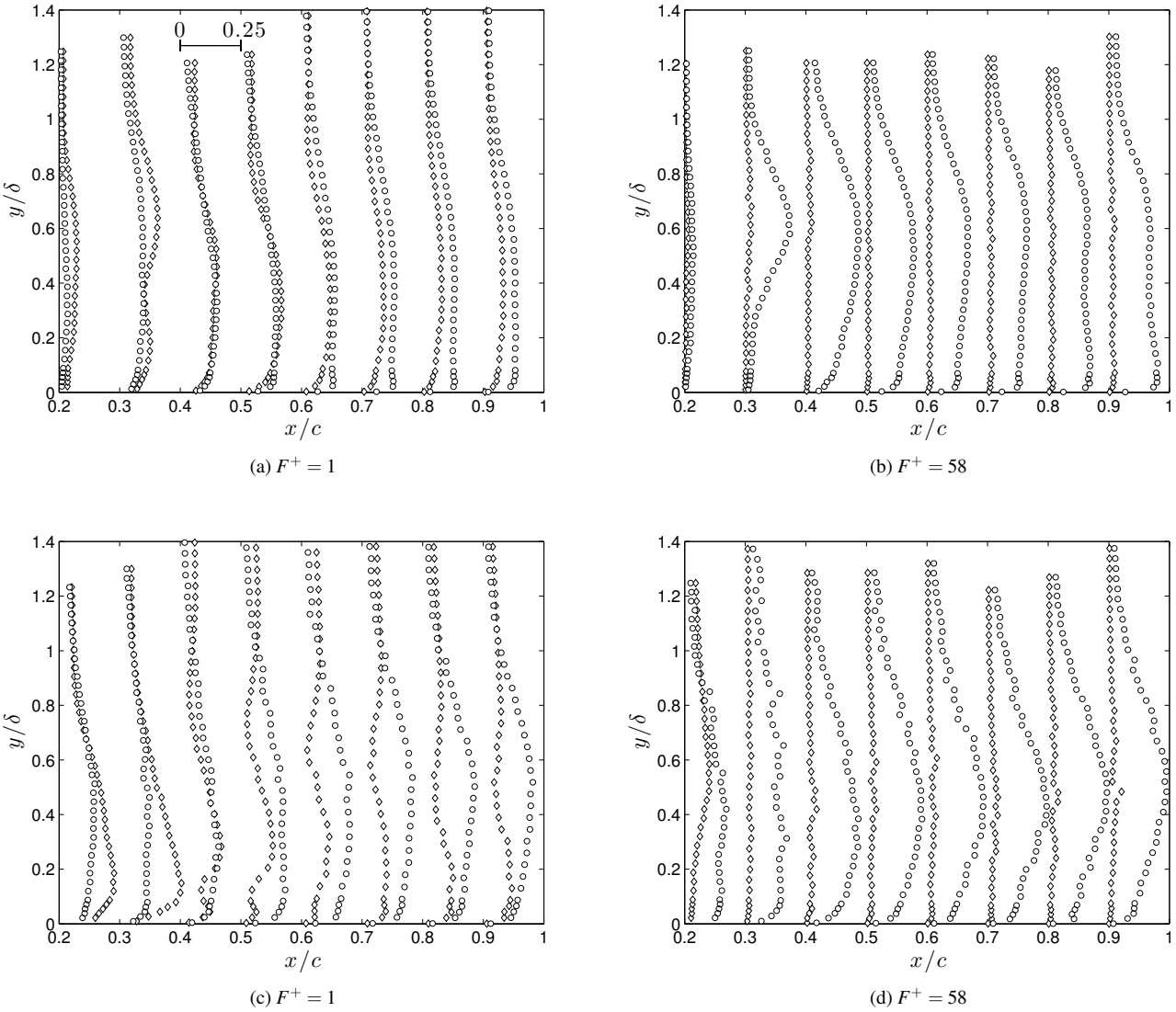


(a) $F^+ = 1$

(b) $F^+ = 58$

(c) $F^+ = 1$

(d) $F^+ = 58$

Figure 7: Coherent and turbulent RMS velocity profiles at $x_j^* = -4.3\%$ (a, b) and $x_j^* = 4.3\%$ (c, d). ($\Diamond$) $\tilde{u}_{\text{rms}}/U_\infty$, ($\circ$) $u'_{\text{rms}}/U_\infty$. The scale for the velocity profiles is given in (a).